Ann. Phys. (Leipzig) **10** (2001) 1–2, 61 – 74

Photoemission spectroscopy in solids

T.-C. Chiang[1], **F. Seitz**[2]

[1]Department of Physics, University of Illinois, 1110 West Green Street
Urbana, IL 61801-3080, USA
[2]Materials Research Laboratory, University of Illinois, 104 South Goodwin Avenue
Urbana, IL 61801-2902, USA
T-Chinag@uiuc.edu

Received 2 Aug. 2000, accepted 29 Sep. 2000 by C. Thomsen

Abstract. The photoelectric effect was discovered and explained in terms of quantum physics about a hundred years ago. Today, photoemission spectroscopy using vacuum ultraviolet radiation and x-rays is an important tool for studying the electronic properties and atomic structure of solids. This paper reviews the development of an understanding of the photoemission process and the basic applications of photoemission spectroscopy in solids, including band structure determination, studies of quasiparticle properties, and core level spectroscopy.

Keywords: photoemission, photoelectron, spectroscopy, band structure, solids
PACS: 79.60, 71.20

1 Introduction

The photoelectric effect was discovered in 1887 by H. Hertz in a study of electric sparks across gaps [1]. He observed that sparks could be triggered by ultraviolet illumination generated by a nearby spark. This illumination was shown to lead to electron emission that aided spark formation. A quantitative explanation for the ensuing observations of light-induced electron emission was given by Albert Einstein in 1905 [2], whose theory of the photoelectric effect was a cornerstone for modern quantum mechanics. He was awarded the Nobel Prize in 1921 for this work. Two important concepts were introduced by his theory. First, light is made of quanta (photons), and the energy of each photon is given by the product of Planck's constant and the frequency of the light $h\nu$. Second, an electron can absorb a photon and emit with the full final energy.

It was later recognized that such electron emission carried useful information about the electronic structure of solids [3–8]. Since the mean free path of photoelectrons ranges typically from a few Ångströms to a few tens of Ångströms, photoemission measurements are surface sensitive. Early experiments were troubled by contamination and the uncertain states of the sample surface. It took about 50 years after Einstein's theory before the widespread deployment of ultrahigh vacuum techniques in research that allowed experiments on samples sufficiently clean to yield reproducible and meaningful results. Both surface and volume effects were reported in experimental

and theoretical studies, and there was much confusion about the relative importance of these effects in the early years.

In the 1960's synchrotron radiation sources became available [4, 9], which spurred a rapid development and growth of photoemission as a major research field. The continuous tunability over a wide energy range and high intensity from such sources facilitated experiments on a variety of systems, including solids, surfaces, and adsorbates. Another important development was highly efficient electrostatic electron energy analyzers that allowed detection of the typically fairly weak photoemission signal within a reasonable time. Concomitant to the rapid expansion in experimental effort, theories were developed to explain the photoemission results in terms of basic electronic properties and atomic structure of solids and surfaces.

Today, third-generation synchrotron radiation sources equipped with magnetic insertion devices (undulators and wigglers) offer unprecedented brightness, and plans are already underway for fourth-generation machines and free-electron lasers. For some materials, the beam intensity available now is already high enough to cause damage. As for the detectors, two-dimensional or multi-channel detection has become commonplace. Compared with early experiments with an energy resolution of $\sim$ 1 eV and an angular resolution of a few degrees, modern instruments are orders of magnitude better, with energy resolution of $\sim$ 1 meV and angular resolution approaching 0.01°. These capabilities allow highly precise measurements of subtle effects that go beyond the usual single-particle picture, providing critical tests of the foundation of many-body quantum theory including the interactions of electrons (or quasiparticles) among themselves and with other elementary and collective excitations. These capabilities also set stringent limits on levels of impurity and imperfection in materials that can be tolerated. Impurities and defects near a surface tend to smear out spectral features, and efforts to improve resolution further would be useless unless the materials of interest can be prepared with correspondingly improved quality. Materials preparation and control at the atomic level is indeed an important emphasis in modern materials research.

This article reviews the development and status of some important basic topics of photoemission spectroscopy in solids, including band structure determination, studies of quasiparticle properties, and core level spectroscopy. Limited by space, this review has to be selective, and the selection is to emphasize basic concepts in solid state physics based on the quantum theory.

2 Photoemission from Valence Electrons

Valence electrons are found within $\sim$ 10 eV of the Fermi level. They are responsible for the chemical bonding of atoms in a solid. A basic description of these electronic states is the band structure, which is of central importance to solid state physics. Despite the many advances made in theoretical band structure calculations over the years, there were no experimental methods for band mapping, or direct determination of the band structure, until the advent of angle-resolved photoemission and development of a good understanding of the photoemission process. Figure 1 shows the typical experimental geometry. The energy of the photon $h\nu$ can range from a few eV to over a thousand

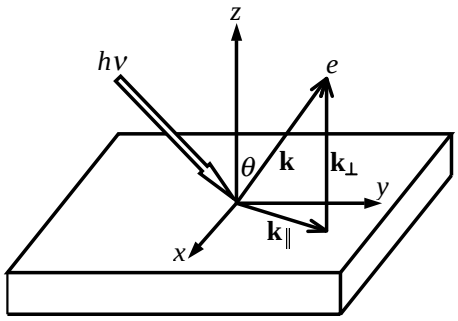

Fig. 1 A schematic showing the angle-resolved photoemission geometry. $h\nu$ is the photon energy, and θ is the polar emission angle.

eV. At low photon energies, as employed in most studies, the momentum of the photon is negligible compared to the crystal momentum. Dipole transitions dominate, and the electric field polarization, the surface normal, and the crystallographic directions in the sample determine the selection rules and transition probabilities. The kinetic energy of the photoelectron E_k is the quantity measured, from which one can deduce the wave vector of the photoelectron $k = \sqrt{2mE_k}/\hbar$ and the binding energy of the initial state $E_b = h\nu - E_k - \phi$, where ϕ is the work function. The component of k parallel to the surface, $k_\parallel$, is conserved throughout the photoemission process, within a surface reciprocal lattice vector, provided that the surface is well ordered. The component perpendicular to the surface, $k_\perp$, is not necessarily conserved, because the surface breaks the translational symmetry. As a result, $k_\perp$ is generally unknown, and this "$k_\perp$ is generally problem" has been a major issue for band mapping. A normal-emission geometry is often employed for simplicity, for which $k_\parallel = 0$, and E_b as a function of $k_\perp$ is the quantity of interest.

3 Band mapping

Figure 2 illustrates the basics of band mapping and the origin of the "$k_\perp$ problem". A set of normal-emission spectra from Ag(111) taken with $h\nu = 7, 8$, and 9 eV is shown, together with a band diagram [10]. The sharp peak just below the Fermi level does not disperse as a function of $h\nu$, and is derived from a Shockley surface state within the band gap at the zone boundary [11]. The other peak at higher binding energy shifts as a function of $h\nu$, and is derived from a bulk band-to-band transition, or "direct transition". The band structure diagram shows where the transitions occur in the Brillouin zone. These transitions are "vertical", because the photon momentum is negligible. The direct-transition peaks in the photoemission spectra are at binding energies consistent with the band diagram. However, the band structure cannot be deduced from the photoemission results alone because of the lack of information about $k_\perp$. All one learns from the measurement is the binding energy for a given photon energy. Early band mapping studies relied on an assumed or calculated find band

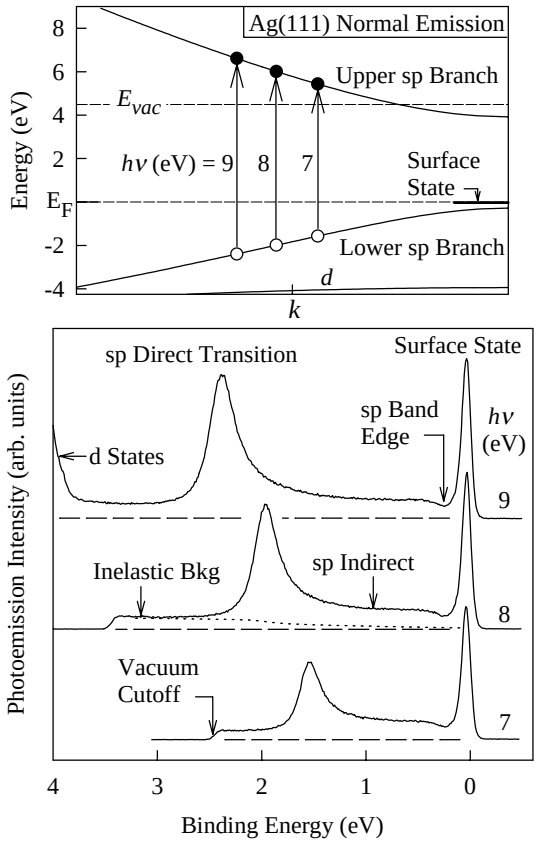

Fig. 2 The bottom panel shows normal-emission spectra from Ag(111) taken with $h\nu = 7, 8,$ and 9 eV, and the spectral features are labeled. The top panel shows the relevant band structure along [111]. The arrows indicate direct transitions.

dispersion relation to fix this $k_\perp$ problem, and in favorable cases this approach could be improved by various interpolation schemes or consistency checks.

A model-independent, direct, and general method is now available, as illustrated by the results in Fig. 3. Here, a set of normal-emission spectra taken from cleaved GaAs(110) is shown together with a band diagram [12]. The energies of the photons are relatively high in this case, and one would expect a great many final bands, which are lifetime broadened to form essentially a continuum. If the transition matrix element were the same for all final bands, there would not be any $k_\perp$-selection, and the results should resemble the one-dimensional density of states along the surface-normal direction. The data, however, clearly show four major dispersive peaks (labeled 1-4), which could be identified with the four valence bands in GaAs. It turns out that the transition matrix element is not uniform at all, but heavily favors those final states with $E(k_\perp)$ near a free-electron dispersion shifted by the inner potential (the average

potential inside a crystal). It is this Fourier component of the wave function inside the crystal that couples strongly to the detector. The high energy of the final state is key to this simplification. The crystal potential that causes umklapp transitions (or mixing of the Fourier components in other directions) becomes a minor perturbation. To first order, the crystal can be treated as a jellium, and thus the free-electron approximation (or the Sommerfeld model) works. The only first-order effect of the crystal potential is surface refraction by the inner potential.

The band structure of GaAs along [110] determined within this free-electron approximation is shown in the bottom panel of Fig. 3 as circles. The results are in good agreement with a calculated band structure indicated by the curves. This band diagram is plotted with the binding energy as the horizontal axis to illustrate the similarity between the band dispersion relations and the peak movements as indicated by the dashed curves over the data. As the photon energy increases, $k_\perp$ increases monotonically in the extended zone, and the peaks follow the dispersion curves from the zone center to the boundary and then back, etc.

This method can be easily generalized to arbitrary emission directions for band mapping over the entire Brillouin zone. The band structure of GaAs along three major crystallographic directions is shown in Fig. 4 as an illustration [12]. Note that there are additional weak features in the spectra shown in Fig. 3 that represent higher-order effects not accounted for by the free-electron approximation. Some of these are non-dispersive, and are associated with critical points with high state densities, as marked in the figure.

4 Surface photoemission

By the early 1980's, the issue of band mapping was considered solved. A large collection of experimental band structures can be found in the literature [8]. However, photoemission peaks from bulk crystals are generally quite broad, and the line shapes are often strange. With the continued improvement in resolution and reproducibility of results by different groups, one could no longer brush aside such observations as caused by experimental problems. To account for the strange-looking line shapes and additional features, it is necessary to consider the effects of the surface. Due to the short mean free path, the surface must play a role other than just supporting some surface states.

The interaction of light with electrons is governed by the interaction Hamiltonian proportional to $\boldsymbol{p}\cdot\boldsymbol{A}+\boldsymbol{A}\cdot\boldsymbol{p}=\boldsymbol{2A}\cdot\boldsymbol{p}-i\hbar\Delta\cdot\boldsymbol{A}$, where $\boldsymbol{A}$ is the vector potential. The $\Delta\cdot\boldsymbol{A}$ term is usually ignored by an appropriate choice of gauge [3,5]. The remaining $\boldsymbol{A}\cdot\boldsymbol{p}$ term gives rise to $\boldsymbol{k}$-selective vertical optical transitions at low energies. However, at a surface, the $\Delta\cdot\boldsymbol{A}$ term cannot be ignored. The dielectric discontinuity gives rise to a corresponding discontinuity in $A_\perp$, which upon differentiation, yields a delta function at the surface. As a result, the matrix element between any initial and final states $\langle\Psi_f|\nabla\cdot\boldsymbol{A}|\Psi_i\rangle$ is nonzero provided both states have a non-zero amplitude at the surface. This surface photoemission term is thus non-selective in $k_\perp$, and the resulting spectrum in normal emission should resemble a one-dimensional joint density of states. This explains why density-of-states features are often observed.

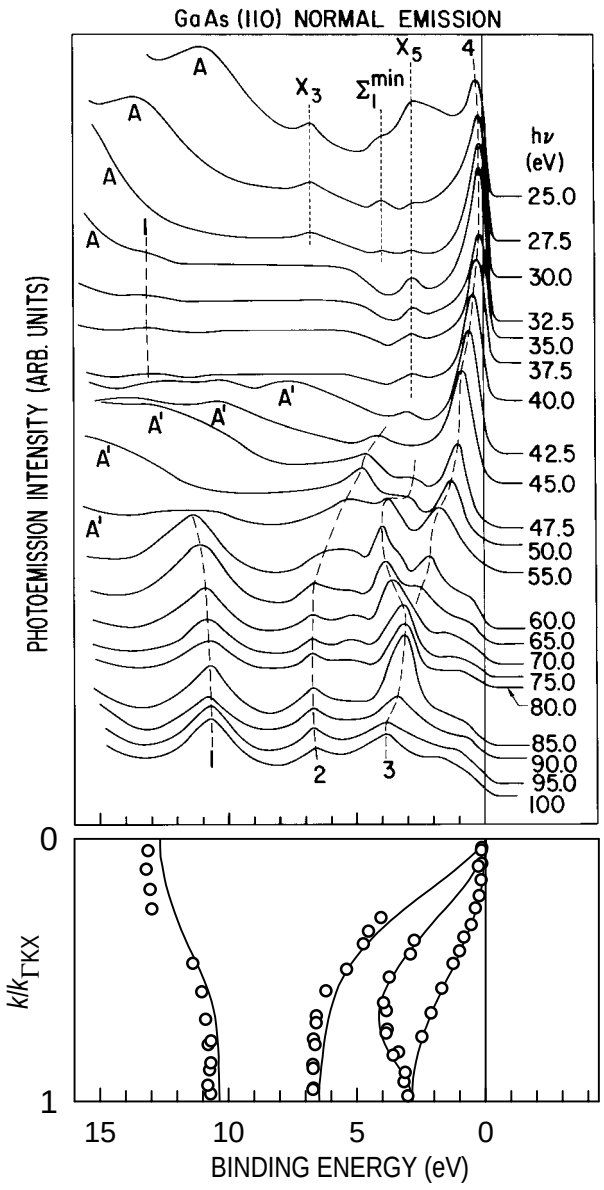

Fig. 3 The top panel shows normal-emission spectra taken from cleaved GaAs(110) for various photon energies as indicated. The dashed curves indicate the dispersions of the valence peaks. The features A and A' are Auger transitions derived from the Ga and As core levels, respectively. The vertical dotted lines indicate density-of-state features as labeled. The bottom panel shows the experimental (circles) and theoretical (curves) band structure along [110].

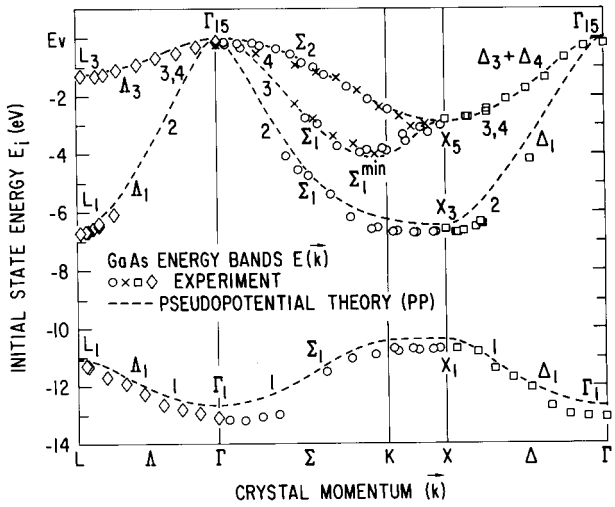

Fig. 4 Experimental (symbols) and theoretical (curves) band structure of GaAs along the major symmetry directions.

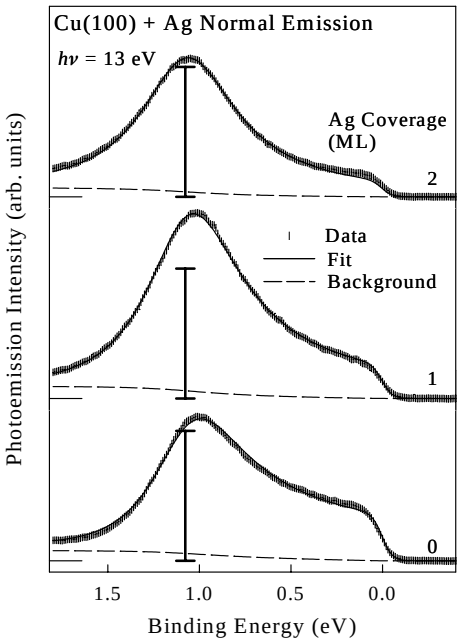

Fig. 5 Normal-emission spectra from clean Cu(100) and Cu(100) covered by 1 and 2 ML of Ag taken with a photon energy of 13 eV. The vertical I bars under the peaks, drawn with the same height at the direct-transition energy, are used to highlight the variations in peak height and asymmetry. The dashed curves indicate the background function for each spectrum.

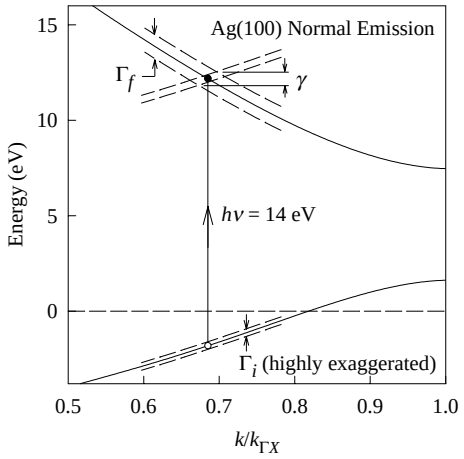

Fig. 6 Band diagram for Ag(100). The vertical arrow indicates a direct transition at a photon energy of 14 eV. The horizontal dashed line is at the Fermi level. The lifetime broadening of each band is indicated schematically by the dashed curves parallel to the band.

The photoemission spectrum is, however, not a simple sum of the bulk and surface intensities. The total matrix element, proportional to $\langle \Psi_f | 2\boldsymbol{A}\cdot\boldsymbol{p} - i\hbar\nabla\cdot\boldsymbol{A}|\rangle$, involves a phased sum of the two contributions. Upon squaring to yield the intensity, there can be an interference effect between the bulk contribution, which is a peak by itself, and the surface contribution, which is generally a continuum spanning the entire valence band [10]. The result is then a Fano-like profile. The spectra in Fig. 2 offer an example; each direct-transition peak is obviously asymmetric. The bulk and surface contributions interfere constructively on the low binding energy side, giving rise to a broad emission plateau, traditionally known as the indirect-transition plateau, which extends towards lower binding energies all the way to the band edge near the surface state. On the high binding energy side of the direct-transition peak, the intensity is much lower due to destructive interference.

Figure 5 shows another example [13]. Here, the bottom spectrum is from Cu(100), and the direct-transition peak is again asymmetric due to interference with surface photoemission. The surface contribution can be eliminated by covering the surface with a carefully chosen overlayer, Ag(111) in the present case. As shown by the other two spectra, the line shape evolves with Ag coverage, and becomes fairly symmetric at a coverage of two monolayers. This symmetric line shape approximately reflects the line shape from the bulk transition alone, and is well represented by a Lorentzian with a width determined by lifetime. In some extreme cases, the interference effect can be sufficiently strong that the direct-transition peak appears missing or in very different energy positions [14]. Data interpretation must be done with great care to avoid erroneous conclusions.

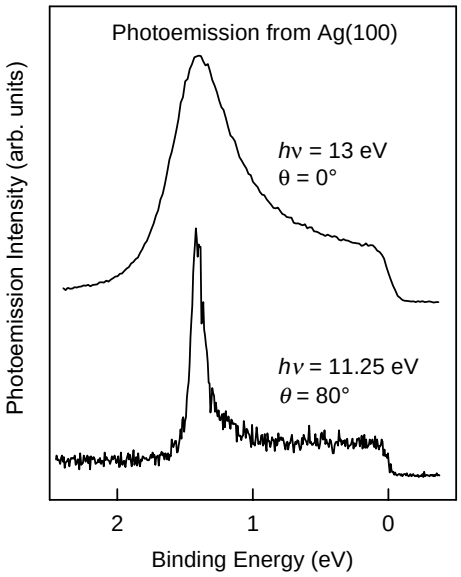

Fig. 7 Angle-resolved photoemission spectra taken with a normal-emission geometry (top curve) and a grazing-emission geometry (bottom curve). The photon energies, indicated in the figure, are chosen to yield a direct-transition peak at about the same binding energy.

5 Line widths and quasiparticle lifetimes

Figure 5 shows that the direct-transition peak, with the surface contribution removed, is quite broad. This width is dominated by the final-state contribution. Figure 6 shows schematically the contributions from the initial and final states for normal emission from Ag(100). The lifetime-broadened initial band, translated up by the photon energy, overlaps with the much broader final band. The width of the overlapping region, γ, is the measured width. The width of the initial state, or the quasi-particle inverse lifetime Γ_i, is too small to be extracted reliably from such measurements. An actual spectrum for normal emission from Ag(100) is shown in Fig. 7 (upper curve) to illustrate the wide width. Again, the line shape is asymmetric due to surface photoemission.

The lower spectrum in Fig. 7 is also from Ag(100), but taken at a grazing emission direction ($\theta = 80°$) and a different photon energy chosen to yield about the same initial-state energy (and hence about the same initial-state lifetime width). The peak is much narrower. The particular combination of photon energy and emission direction eliminates the final-state contribution to the width, while at the same time the initial-state contribution is compressed by about a factor of two. In other words, the measured peak width, after accounting for instrumental resolution, is about one half of the width of the quasiparticle inverse lifetime. Although somewhat counterintuitive, this line width compression does not violate quantum mechanics [15]. The photoemission spectrum is measured as a function of binding energy, which is related to the

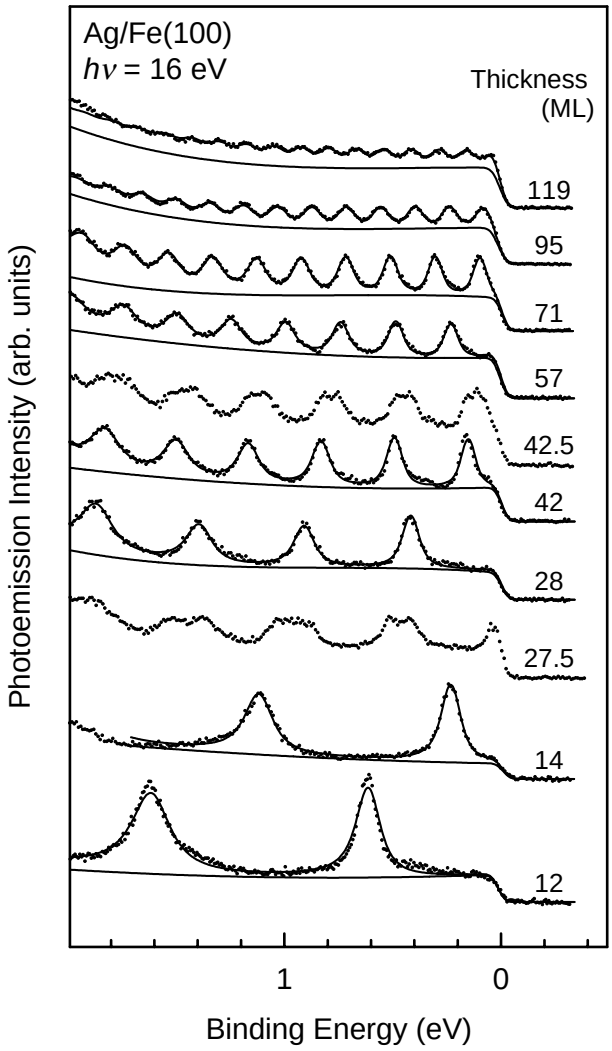

Fig. 8 Normal emission spectra for Ag deposited on Fe(100) at various coverages as indicated. The photon energy is $h\nu = 16$ eV. The data points are shown as dots, while the fits to the data and the background functions are shown as curves. The peaks are derived from quantum well states.

momentum by a kinematic relation. Thus, different binding energies correspond to different momenta. If the measurement were carried out at a fixed $\boldsymbol{k}$, the observed energy width would be a direct measure of the lifetime width. This could be done in a different photoemission mode – the "constant-final-state mode". In the usual mode of photoemission as the case shown in Fig. 7, each point in a spectrum corresponds to a different $\boldsymbol{k}$, and this effect can become quite significant at grazing emission, where variation in $k_{\|}$ across a peak can give rise to either peak compression or expansion.

6 Surfaces, films, and systems of lower dimensions

As exemplified by the case of Ag(111) (Fig. 2), surface states are usually much sharper than bulk states in photoemission. The reason for this sharpness is that there is no final-state contribution because the transition does not involve $k_{\perp}$ (see Fig. 6). Surface states are specified by $k_{\|}$ only, which is rigorously conserved for a periodic system, and the lifetime of the final free-electron state entering the detector is practically infinite. Also, the wave function of a surface state can be spatially decoupled from the bulk, and decay channels that affect bulk states become restricted or diminished. Surface states, because of their narrow peak widths and simplicity (no $k_{\perp}$), have been a popular choice for photoemission studies, especially in high-resolution work.

Likewise, nearly-two-dimensional systems, such as layer compounds, as well as quasi-one-dimensional systems, are popular subjects for high-resolution work. In these systems, there is an increased overlap of electronic wave functions due to geometrical confinement, possibly resulting in increased electron correlation. If the bandwidth of the material is small, the electronic structure can deviate significantly from the traditional Fermi liquid or band behavior, and exotic phases can result. A well-known example is the high-temperature superconductors, for which there has been a large effort worldwide to understand the photoemission results. For one-dimensional systems, there is much current interest in the Luttinger-liquid behavior. Some of the results are still controversial, and clearly much more research is needed to clarify the many-body physics underlying the complex phenomena exhibited by low-dimensional, small-band-width systems.

Returning to the subject of bulk band structure determination in traditional materials, there is yet a different, direct method that offers a much higher accuracy. This method relies on the use of thin films. Figure 8 shows a set of normal-emission spectra taken from Ag(100) films grown on Fe(100) [16]. The periodic peaks are unique to the thin film configuration, and represent quantum-well states for Ag electrons confined in the film by the boundary potential. These states are analogues to those described in quantum mechanics textbooks for a particle confined in a potential well. Or, one can interpret them as Fabry-Pérot modes in an electron interferometer. Note that all of the films with integer monolayer coverages show sharp peaks. The spectrum for a coverage of 27.5 monolayers (ML) shows a linear combination of two sets of peaks, one corresponding to 27 ML, and the other 28 ML. Likewise, the spectrum for 42.5 ML exhibits two sets of peaks corresponding to the two neighboring integer layer thicknesses. Such atomic layer resolution illustrates that all of the other spectra correspond to atomically uniform films. Starting from a clean surface, one can add small amounts

of Ag to build up a film one monolayer at a time, and this layer counting provides an absolute determination of film thicknesses over a wide range.

Using such atomically uniform films, one can deduce the band structure and quasiparticle lifetime from the measured peak positions and peak widths. The peak positions are determined by the interferometer modes, or standing wave patterns in the film. Since the film thicknesses are quantized in terms of the atomic layer thickness, the resulting band structure is very accurate. Results for Ag(100) yield a Fermi wave vector accurate to $\sim 0.1\%$, which challenges the traditional de Haas-van Alphen measurement. The measured lifetime width as a function of temperature, film thickness, and binding energy can be analyzed to yield separate contributions from electron-electron scattering, electron-phonon scattering, and electron-defect scattering [16].

7 Photoemission from core electrons

Limited by surface, only brief remarks will be made here. Core levels are deeply bound, atomic-like states, and show little band dispersions. They require higher energy photons for excitation, and hence the technique is often referred to as x-ray photoelectron spectroscopy (XPS). Kai Siegbahn's group pioneered the field, for which he was award the Nobel Prize in 1981. Emission from each core level gives rise to a peak with a unique energy, which is suitable for chemical analysis. As the instrumental resolution and sensitivity improved, it was noticed that core level emission from metals gave rise to an asymmetric line shape, which was later understood as arising from the many-body response of a Fermi liquid to a sudden creation of a core hole. Also noticed early on were satellite features due to shake-up transitions involving the excitations of other electrons or plasmons. Studies of these phenomena contributed much to the development of many-body physics [3, 5, 7].

An important scientific and industrial application of XPS is analysis of surface composition, also known as Electron Spectroscopy for Chemical Analysis (ESCA). Many commercial machines are employed in industrial and academic research laboratories worldwide. With sufficient resolution and in favorable cases, one can distinguish different chemical states of a given element as revealed by shifts of core level peak positions [17]. Such chemical shifts are often analyzed in terms of initial-state effects, including charge transfer, and final-state screening effects. Beginning in the late 1970's and early 1980's, the experimental resolution became high enough that intrinsic surface core level shifts for films and single-crystal substrates were detected [18, 19]. Different surface reconstructions of the same material can exhibit different core level shifts, and this information is useful for understanding the relationships between the surface atomic structure and electronic properties.

It was noticed in early work that core level intensities vary as a function of emission direction and photon energy. Some of these variations reflect the properties of the core level wave function. Additional variations are due to final-state effects, including diffraction. A core electron emitted from an atom is represented by a wave, and can be scattered by nearby atoms. If the emission is from a surface atom on a crystal, one can visualize this as a wave emanating from a point source being scattered or diffracted by the underlying three-dimensional crystal structure. Since the mean free path of

the photoelectron is rather short, only nearby atoms contribute significantly to the diffraction process. Nevertheless, multiple scattering is important, and early studies often employed a fitting procedure starting from an assumed model. The methodology is in many ways similar to that employed in low energy electron diffraction [20].

In the past decade or so, there has been an increased understanding of the diffraction process as well as an increased efficiency in data acquisition and analysis that has led to the development of photoelectron holography [21]. In this approach, a large set of intensity data taken over many emission directions and excitation photon energies is used as a hologram for direct mathematical inversion to yield an image of atoms near the emitter. This model-independent, direct approach holds great promise for routine structural analysis. An important, related development is the extended fine-structure measurement similar to EXAFS, which allows atomic bond-length determination.

8 Concluding remarks and outlook

Photoemission has a long history, with its evolution intimately tied to the development of quantum mechanics. Interaction of light with solids and the resulting emission of electrons is a complex phenomenon. Each major improvement in experimental capabilities has led to observations of new phenomena and finer details that require a deeper understanding of the underlying physics. This brief review focuses on the basics of photoemission and its applications in fundamental scientific studies of solids. Space limitations forced the omission of many important subjects, such as spin-resolved, time-resolved, spatially-resolved, and multi-photon photoemission. As photon sources and electron analyzers become more powerful and more sophisticated, there will undoubtedly be many more discoveries and surprises. Current emphasis on electron correlation effects should lead to a detailed understanding of the many intriguing aspects of many-body physics, and such understanding is important for the design and application of "complex functional materials" for future generations of devices. For fundamental scientific research, we hope that one day we would be able to perform time-, spin-, and angle-resolved photoemission from a single specific atom in a solid, thus yielding a complete specification of the electronic and magnetic properties, atomic structure, and dynamic behavior.

Acknowledgements

Much of the material presented here is based upon work supported by the U. S. National Science Foundation, under Grant Nos. DMR-99-75470 and DMR-99-75182, the U. S. Department of Energy, Division of Materials Sciences, under Grant No. DEFG02-91ER45439, and the Donors of the Petroleum Research Fund, administered by the American Chemical Society. The Synchrotron Radiation Center of the University of Wisconsin, where much of the work was performed, is supported by the National Science Foundation under Grant No. DMR-95-31009.

References

[1] H. Hertz, Ann. Physik **31** (1887) 983
[2] A. Einstein, Ann. Physik **17** (1905) 132
[3] *Photoemission in Solids I*, edited by M. Cardona and L. Ley, Topics in Applied Physics, Vol. 26, Springer, Berlin, 1978
[4] *Photoemission in Solids II*, edited by M. Cardona and L. Ley, Topics in Applied Physics, Vol. 27, Springer, Berlin, 1979
[5] *Photoemission and the Electronic Properties of Surfaces*, edited by B. Feuerbacher, B. Fitton, and R. F. Willis, Wiley, New York, 1978
[6] *Angle-resolved Photoemission*, edited by S. D. Kevan, Studies in Surface Science and Catalysis, Vol. 74, Elsevier, Amsterdam, 1992
[7] S. Hüfner, *Photoelectron Spectroscopy - Principles and Applications*, Springer Series in Solid-State Science, Vol. 82, Springer, Berlin, 1995
[8] *Electronic Structure of Solids: Photoemission Spectra and Related Data*, edited by A. Goldmann and E. E. Koch, Landolt-Börnstein, Numerical Data and Functional Relationships in Science and Technology, New Series, Group III, Vol. 23, Springer, Berlin, 1989
[9] G. Margaritondo, *Introduction to Synchrotron Radiation*, Oxford University Press, New York, 1988
[10] T. Miller, W. E. McMahon, and T.-C. Chiang, Phys. Rev. Lett. **77** (1996) 1167; T. Miller, E. D. Hansen, W. E. McMahon, and T.-C. Chiang, Surf. Sci. **376** (1997) 32
[11] P. O. Gartland and B. J. Slagsvold, Phys. Rev. B **12** (1975) 4047
[12] T.C. Chiang, J. A. Knapp, D. E. Eastman, and M. Aono, Solid State Commun. **31** (1979) 917; T.C. Chiang, J. A. Knapp, M. Aono, and D. E. Eastman, Phys. Rev. B **21** (1980) 3513
[13] E. D. Hansen, T. Miller, and T.-C. Chiang, Phys. Rev. Lett. **78** (1997) 2807
[14] D. Claesson, S.-Å. Lindgren, L. Walldén, and T.-C. Chiang, Phys. Rev. Lett. **82** (1999) 1740
[15] E. D. Hansen, T. Miller, and T.-C. Chiang, Phys. Rev. Lett. **80** (1998) 1766
[16] J. J. Paggel, T. Miller, and T.-C. Chiang, Science **283** (1999) 1709; Phys. Rev. Lett. **83** (1999) 1415; Phys. Rev. B **61** (2000) 1804
[17] S. Hagström, C. Nordling, and K. Siegbahn, Z. Physik **178** (1964) 439
[18] P. H. Citrin, G. K. Wertheim, and Y. Baer, Phys. Rev. Lett. **41** (1978) 1425
[19] D. E. Eastman, T.C. Chiang, P. Heimann, and F. J. Himpsel, Phys. Rev. Lett. **45** (1980) 656
[20] A. Liebsch, Phys. Rev. Lett. **32** (1974) 1203
[21] A. Szöke, in *Short Wavelength Coherent Radiation: Generation and Applications*, edited by D. T. Attwood and J. Bokor, AIP Conf. Proc. No. 147, American Institute of Physics, New York, 1986; J. J. Barton, Phys. Rev. Lett. **61** (1988) 1356